

NAS-Count: Counting-by-Density with Neural Architecture Search

Yutao Hu¹, Xiaolong Jiang¹, Xuhui Liu¹, Baochang Zhang¹, Jungong Han²,
Xianbin Cao¹, David Doermann³

¹Beihang University, ²University of Warwick, ³State University of New York, Buffalo

Abstract

Most of the recent advances in crowd counting have evolved from hand-designed density estimation networks, where multi-scale features are leveraged to address scale variation, but at the expense of demanding design efforts. In this work, we automate the design of counting models with Neural Architecture Search (NAS) and introduce an end-to-end searched encoder-decoder architecture, Automatic Multi-Scale Network (AMSNet). The encoder and decoder in AMSNet are composed of different cells discovered from counting-specific search spaces, each dedicated to extracting and aggregating multi-scale features adaptively. To resolve the pixel-level isolation issue in training density estimation models, AMSNet is optimized with a novel Scale Pyramid Pooling Loss (SPPLoss), which exploits a pyramidal architecture to achieve structural supervision at multiple scales. During training time, AMSNet and SPPLoss are searched end-to-end efficiently with differentiable NAS techniques. When testing, AMSNet produces state-of-the-art results that are considerably better than hand-designed models on four challenging datasets, fully demonstrating the efficacy of NAS-Count.

1. Introduction

Given crowded images, a crowd counting model estimates the number of people contained in a given area. If performed accurately, this has far-reaching applications in crowd monitoring, urban planning, traffic management, and disaster relief [57, 51, 52]. With advanced occlusion robustness and counting efficiency, counting-by-density [29, 75, 10, 25] has become the method-of-choice over others related techniques [30, 21, 12, 24, 12]. These techniques estimate a pixel-level density map and count the crowd by summing over pixels in the given area.

Although effective, counting-by-density is still challenged with scale variations induced by perspective distortion. As illustrated in Figure.1, the scales of people vary inversely with their distances to the camera causing an inconsistent crowd distribution in the density map. To ad-

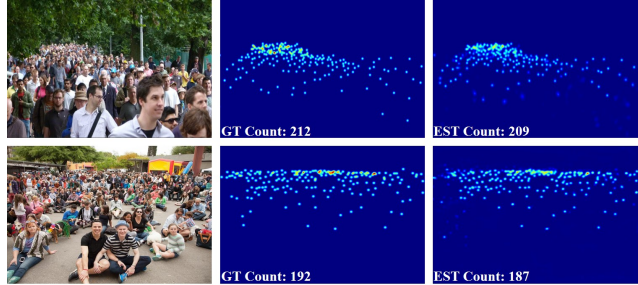


Figure 1. A demonstration of the scale variation issue in the counting-by-density task. Due to varied distances to the camera, objects are perspectively distorted in the input with varied scales.

dress this issue, most methods [75, 10, 40] employ deep Convolutional Neural Network (CNN) for exploiting multi-scale features to perform density estimation in multi-scaled scenes. In particular, different-sized filters are arranged in parallel in multiple columns to capture multi-scale features for accurate counting in [75, 44, 53], while in [10, 25, 26], different filters are grouped into blocks and then stacked sequentially in one column. At the heart of these solutions, multi-scale capability originates from the compositional nature of CNNs [7, 67], where convolutions with various receptive fields are composed hierarchically by hand. However, these manual designs demand prohibitive expert-efforts and suffer from heuristically-fixed receptive fields.

We therefore developed a Neural Architecture Search (NAS) [77, 48] based approach to automatically discover multi-scaled counting-by-density models. NAS is enabled by the compositional nature of CNN and guided by human expertise in designing task-specific search space and strategies. For vision tasks, NAS blooms with image-level classification [78, 35, 47, 46], where novel architectures are found to progressively transform spatial details to semantically deep features. Counting-by-density is, however, a pixel-level task that requires spatial preserving architectures with refrained down-sampling strides. Accordingly, the successes of NAS in image classification are not immediately transferable to crowd counting. Although attempts have been made to deploy NAS in image segmentation for

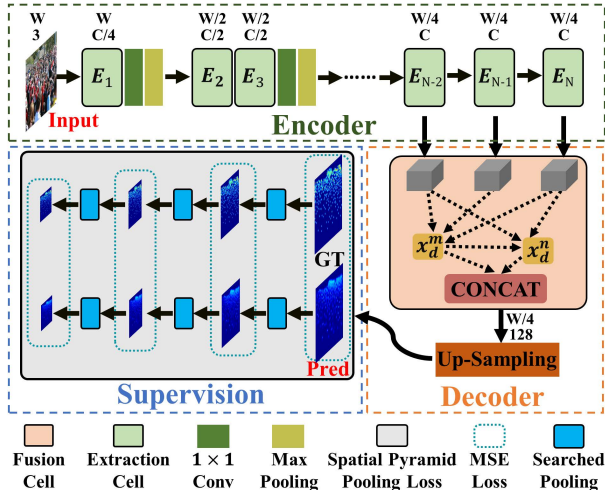


Figure 2. An illustration of NAS-Count with the AMSNet architecture and SPPLoss supervision, all searched cells are outlined in black. Given $W \times W \times C$ ($C = 3$) inputs, the output dimension of each extraction and fusion cell are marked accordingly.

pixel-level classifications [13, 34, 42], they are still not able to address counting-by-density, which is a pixel-level regression with scale variations across the inputs.

In NAS-Count we propose a counting-oriented NAS framework with specific search space, search strategy, and supervision method, what we use to develop our Automatic Multi-Scale Network (AMSNet). First, we employ a two-level search space [54, 34]. On the micro-level, multi-scaled cells are automatically explored to extract and fuse multi-scale features sufficiently. Pooling operations are limited to preserve spatial fidelity and dilated convolutions are utilized instead for receptive field enlargement. On the macro-level, multi-path encoder-decoder architectures are searched to produce a high-quality density map. Fully-convolutional encoder-decoder is the architecture-of-choice for pixel-level tasks [49, 71, 10], and the multi-path variant can better aggregate features encoded at different scales [33, 26, 38]. Second, we adopt a differential one-shot search strategy [37, 34, 70] to improve search efficiency, wherein architecture parameters are jointly optimized with gradient-based optimizer. Third, in order to address the pixel-level isolation problem [10, 31] of the traditional mean square error (MSE) loss, we introduce a novel Scale Pyramid Pooling Loss (SPPLoss) to optimize AMSNet, which leverages a pyramidal pooling architecture to enforce supervision with multi-scale structural awareness. By jointly searching AMSNet and SPPLoss, NAS-Count flexibly exploits multi-scale features and addresses the scale variation issue in counting-by-density. NAS-Count is illustrated in Figure 2.

Main contributions of NAS-Count includes:

- To our best knowledge, NAS-Count is the first attempt

at introducing NAS for crowd counting, where a multi-scale architecture is automatically developed to address the scale variation issue.

- A counting-specific two-level search space is developed in NAS-Count, from which a spatially-preserved encoder-decoder architecture (AMSNet) is discovered efficiently with a differentiable search strategy using stochastic gradient descent (SGD).
- A novel Scale Pyramid Pooling Loss (SPPLoss) is searched automatically to replace MSE supervision, which helps produce the higher-quality density map via optimizing structural information on multiple scales.
- By jointly searching AMSNet and SPPLoss, NAS-Count reports the best overall counting and density estimation performances on four challenging benchmarks, considerably surpassing other state-of-the-arts which all require demanding expert-involvement.

2. Related work

In this section, we briefly review related literature in the domains of crowd counting and neural architecture search.

2.1. Crowd Counting Literature

Existing counting methods can be categorized into counting-by-detection [17, 21, 30, 63], counting-by-regression [11, 50, 24, 74, 28], and counting-by-density strategies. For comprehensive surveys in crowd counting, please refer to [51, 52, 57, 27]. The first strategy is vulnerable to occlusions due to the requirement of explicit detection. Counting-by-regression successfully avoids such requirement by directly regressing to a scalar count, but forfeits the ability to perceive the localization of crowds. The counting-by-density strategy, initially introduced in [29], counts the crowd by first estimating a density map using hand-crafted [29, 20] or deep CNN [75, 31, 64, 39] features, then summing over all pixel values in the map. Being a pixel-level regression task, CNN architectures deployed in counting-by-density methods tend to follow the encoder-decoder formulation. In order to handle scale variations with multi-scale features, single-column [10, 25, 65] and multi-column [75, 5, 44, 62] encoders have been used where different-sized convolution kernels are sequentially or parallelly arranged to extract features. For the decoder, hour-glass architecture with a single decoding path has been adopted [10, 25, 76], while a novel multi-path variant is gaining increasing attention for superior multi-scale feature aggregation [26, 38, 43, 42].

2.2. NAS Fundamentals

Since its inception NAS [77, 48] has been intensively studied with favorable outcomes [19, 72]. The general ef-

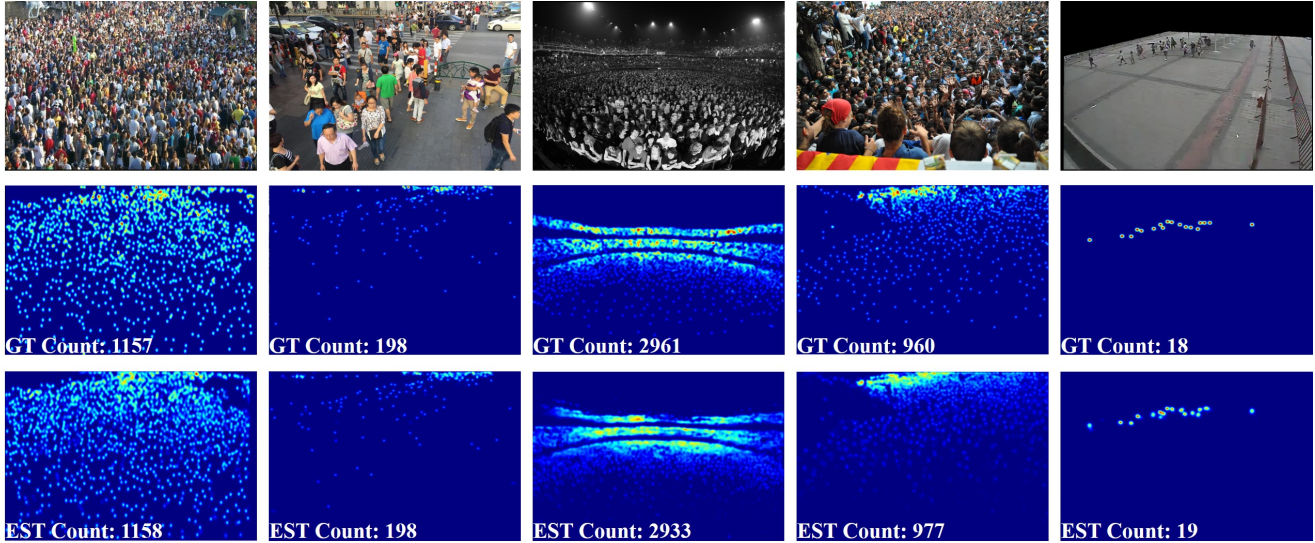


Figure 3. An illustration of generated density maps on ShanghaiTech Part_A, ShanghaiTech Part_B, UCF_50_CC, UCF-QNRF and World-Expo’10 respectively. The first row shows the input images, the second and third depict the ground truth and estimated density maps.

forts of developing new NAS solutions focus on designing new search spaces and search strategies. For search space, existing methods can be categorized into searching the network (macro) space [48, 77], the cell (micro) space [78, 35, 47, 37, 45], or exploring such a two-level space [54, 34] jointly. The cell-based space search is the most popular where the ensemble of cells in networks is hand-engineered to reduce the exponential search space for fast computation. For search strategy, it is essentially an optimizer to find the best architecture that maximizes a targeted task-objective. Random search [4, 23], reinforcement learning [77, 78, 61, 8, 1], neuro-evolutionary algorithms [60, 48, 41, 36, 47, 66], and gradient-based methods [37, 68, 9] have been used to solve the optimization problem, but the first three suffer from prohibitive computation costs. Although many attempts have been made such as parameter sharing [45, 18, 8, 3], hierarchical search [35, 34], deploying proxy tasks with cheaper search space [78] and training procedures [2] to accelerate them, yet they are still far less efficient than gradient-based methods.

Gradient-based NAS, represented by DARTS [37], follows the one-shot strategy [6] wherein a hyper-graph is established using differentiable architectural parameters. Based on the hyper-graph, an optimal sub-graph is explored within by solving a bi-level optimization with gradient-descent optimizers. Noteworthy, this one-shot strategy is inherently memory-heavy, and the bi-level optimization is prone to collapse with excessively-selected skip-connections. These drawbacks of one-shot search strategy are further investigated in DARTS variants including DARTS+ [32], P-DARTS [15], PC-DARTS [70], Single-

Path NAS [59], and AutoDeepLab [34].

2.3. NAS Applications

NAS has shown great promise with discovered recurrent or convolutional neural networks in both sequential language modeling [58] and multi-level vision tasks. In computer vision, NAS has excelled at image-level classification tasks [78, 46, 35, 47], which is a customary starting-point for developing new classifiers outputting spatially coarsened labels. NAS was later extended to both bounding-box and pixel-level tasks, represented by object detection [22, 16, 69] and segmentation [13, 34, 42], where the search spaces are modified to better preserve the spatial information in the feature map. In [13] a pixel-level oriented search space and a random search NAS were introduced to the pixel-level segmentation task. In [42], a similar search space was adopted, but the authors employed a reinforcement learning based search method. Nonetheless, both two methods suffer from formidable computations and are orders of magnitude slower than NAS-Count. In [34], the authors searched a two-level search space with more efficient gradient-based method, yet it dedicates in solving the pixel-level classification in semantic segmentation, which still differs from the per-pixel regression in counting-by-density.

3. NAS-Count Methodology

NAS-Count efficiently searches a multi-scaled encoder-decoder network, the Automatic Multi-Scale Network (AMSN) as shown in Figure 2, in a counting-specific search space. It is then optimized with a jointly searched

Scale Pyramid Pooling Loss (SPPLoss) as shown in Figure 2. The encoder and decoder in AMSNet consist of searched multi-scale feature extraction cells and multi-scale feature fusion cells, respectively, and SPPLoss deploys a two-stream pyramidal pooling architecture where the pooling cells are searched as well. By searching AMSNet and SPPLoss together end-to-end, the receptive fields established in these two architectures can cooperate and collaborate with each other to harvest the ideal multi-scale capability for addressing the scale-varied counting problem. NAS-Count details are discussed in the following subsections.

3.1. Automatic Multi-Scale Network

AMSNet is searched with the differential one-shot strategy in a two-level search space. To address scale variations in the pixel-level counting-by-density problem, we search for a multi-path encoder-decoder architecture, where multi-scale features are adaptively extracted and aggregated. In particular, the down-sampling strides are limited in AMSNet to preserve spatial fidelity. To improve the search efficiency, NAS-Count adopts a continuous relaxation and partial channel connection as described in [70].

3.1.1 AMSNet Encoder

The encoder of AMSNet is composed of a set of multi-scale feature extraction cells. For the l -th cell in the encoder, it takes the outputs of previous two cells, feature maps x_{l-2} and x_{l-1} , as input and produces an output feature map x_l . We define each *cell* as a directed acyclic graph containing N_e nodes, i.e. x_e^i with $1 \leq i \leq N_e$, each represents a propagated feature map. We set $N_e=7$ containing two input nodes, four intermediate nodes, and one output node. Each directed *edge* in a cell indicates a convolutional operation $o_e(*)$ performed between a pair of nodes, and $o_e(*)$ is searched from the search space O_e with 9 operations:

- 1×1 common convolution;
- $3 \times 3, 5 \times 5, 7 \times 7$ dilated convolution with rate 2;
- $3 \times 3, 5 \times 5, 7 \times 7$ depth-wise separable convolution;
- skip-connections;
- no-connection (zero);

For preserving spatial fidelity in the extracted features, extraction cell involves no down-sampling operations. To compensate for the receptive field enlargement, we utilize dilated convolutions to substitute for the normal ones. Besides, we adopt depth-wise separable convolutions to keep the searched architecture parameter-friendly. Skip connections instantiate the residual learning scheme, which helps improving multi-scale capacity as well as enhancing gradient flows during back-propagation.

Within each cell, a specific intermediate node x_e^m is connected to all previous nodes $x_e^1, x_e^2 \dots, x_e^{m-1}$. Edges $o_e^{n,m}(\ast)$ are established between every pair of connected-nodes n and m , forming a densely-connected hyper-graph.

On a given edge $o_e^{n,m}(\ast)$ in the graph, following the continuously-relaxed differentiable search as discussed in [37], its associated operation is defined as a summation of all possible operations weighted by the architectural parameter α_e :

$$o_e^{n,m}(x_e^n; S) = \sum_i \sigma(\alpha_e^{n,m,i}) \cdot o_e^i(S \cdot x_e^n) + (1 - S) \cdot x_e^n, \quad (1)$$

In the above equation, $\sigma(\ast)$ is a softmax function and $i = 9$ indicates the volume of the micro-level search space. Vector S is applied to perform a channel-wise sampling on x_e^n , where $1/K$ channels are randomly selected to improve the search efficiency. K is set to 4 as proposed in [70]. $\alpha_e^{n,m}$ is a learnable parameter denoting the importance of each operation on an edge $o_e^{n,m}(\ast)$.

In addition, each edge is also associated with another architecture parameter $\beta_e^{n,m}$ which indicates its importance. Accordingly, an intermediate node x_e^m is computed as a weighted sum of all edges connected to it:

$$x_e^m = \sum_{n < m} \sigma(\beta_e^{n,m}) \cdot o_e^{n,m}(x_e^n; S) \quad (2)$$

Here n includes all previous nodes in the cell. The output of the cell is a concatenation of all its intermediate nodes. The cell architecture is determined by two architectural parameters α_e and β_e , which are jointly optimized with the weights of convolutions through a bi-level optimization. For details please refer to [37]. To recover a deterministic architecture from continuous relaxation, the most important edges as well as their associated operations are selected by computing *argmax* on $\sigma(\beta_e)$ and $\sigma(\alpha_e)$.

In the encoder, we apply a 1×1 convolution to preliminarily encode the input image into a $\frac{C}{4}$ channel feature map. Afterwards, two 1×1 convolutions are implemented after the first and third extraction cells, each doubling the channel dimension of the features. Our searched extraction cell is normal cell that keeps the feature channel dimension unchanged. Spatially, we only reduce the feature resolution twice with stride two max pooling layers, aiming to preserve the spatial fidelity in the features, while double the channels before the two down-sampling operations. Additionally, within each extraction cell, an extra 1×1 convolution is attached to each input node, adjusting their feature channels to be one-fourth of the cell final output dimension.

3.1.2 AMSNet Decoder

The decoder of AMSNet deploys a multi-scale feature fusion cell followed by an up-sampling module. We construct the hyper-graph of the fusion cell as inputting multiple features while outputting just one, therefore conforming to the aggregative nature of a decoder. The search in this hyper-graph is similar to that of the extraction cell. A fusion cell

takes three encoder output feature maps as input, consisting of $N_f = 6$ nodes that include three input nodes, two intermediate nodes and one output node. After the relaxation as formulated in Eq.1 and 2, the architecture of a fusion cell is determined by its associated architecture parameters α_d and β_d . By optimizing β_d on three edges connecting the decoder with three extraction cells in the encoder, NAS-Count fully explores the macro-level architecture of AMSNet, such that different single- or multi-path encoder-decoder formulations are automatically searched to discover the best feature aggregation for producing high-quality density maps.

As shown in Figure 2, M denotes the number of extraction cells in the encoder and C is the number of channels in the output of the last cell. To improve efficiency, we first employ a smaller proxy network, with $M=6$ and $C=256$, to search the cell architecture. Upon deployment, we enlarge the network to $M=8$ and $C=512$ for better performance. Through the multi-scale aggregation instantiated in the decoder, we obtain a feature map with 128 channels, which is then processed by an up-sampling module containing two 3×3 convolutions interleave with the nearest neighbor interpolation layers. The output of the up-sampling module is a single-channel density map with restored spatial resolution, which is then utilized in computing the SPPLoss.

3.2. Scale Pyramid Pooling Loss

The default loss function to optimize counting-by-density models is the per-pixel mean square error (MSE) loss. By supervising this L_2 difference between the estimated density map and corresponding ground-truth, one assumes strong pixel-level isolation, such that it fails to reflect structural differences in multi-scale regions [10, 31]. As motivated by the Astrous Spatial Pyramid Pooling (ASPP) module designed in [14], we propose to solve this problem of MSE by proposing a new supervision architecture we call the Scale Pyramid Pooling Loss (SPPLoss), where non-parametric pooling layers are stacked into a two-stream pyramid. As shown in Figure 4, after feeding the estimated map E and the ground-truth G into each stream, they are progressively coarsened and MSE losses are calculated on each level between the pooled maps. This is equivalent to computing the structural difference with increasing region-level receptive fields, and can therefore better supervise the pixel-level estimation model on different scales.

Instead of setting the pooling layers manually as in [26], NAS-Count searches the most effective SPPLoss architecture jointly with AMSNet. In this way, the multi-scale capability composed in both architecture can better collaborate to resolve the scale variation problem in counting-by-density. Specifically, each stream in SPPLoss deploys $N_l=4$ cascaded nodes. Among them, one input node is the predicted density map (or the given ground-truth). The other

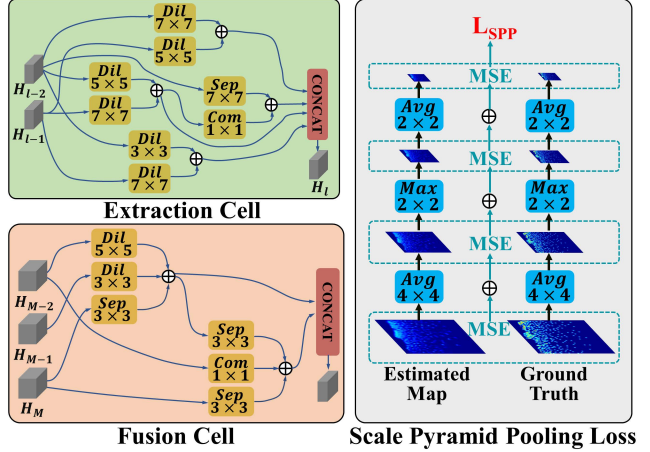


Figure 4. Detailed illustrations of the best searched cells. The circled additive sign denotes element-wise or scalar additions.

three nodes are produced through three cascaded searched pooling layers. The search space for operation O_l performed on each edge contains six different pooling layers including:

- 2×2 , 4×4 , 6×6 max pooling layer with stride 2;
- 2×2 , 4×4 , 6×6 average pooling layer with stride 2;

The search for SPPLoss adopts the similar differentiable strategy as detailed in Section 3.1. Notably, as SPPLoss is inherently a pyramid, its macro-level search space takes a cascaded form instead of a densely-connected hyper-graph. Accordingly, we only need to optimize the operation-wise architecture parameter α_s as follows:

$$o_s^{n,m}(x_s^n) = \sum_i \sigma(\alpha_s^{n,m,i}) \cdot o_s^i(x_s^n) \quad (3)$$

Here, i indexes 6 different pooling operations, and x_s^n represents an estimated map E or ground-truth G in specific level. Since both of them only have one channel, we thus do not apply partial channel connections (*i.e.* set K equals to 1). The same cascaded architecture is shared in both streams of SPPLoss. Using the best searched architecture as depicted in Figure 4, SPPLoss is computed as:

$$L_{SPP} = \sum_n \frac{1}{N^l} \|\phi^l(E) - \phi^l(G)\|_2^2 \quad (4)$$

N^l denotes the number of pixels in the map, $\phi^l(*)$ indicates the searched pooling operation, superscript l is the layer index ranging from 0 to 3. $l = 0$ is the special case where MSE loss is computed directly between E and G .

4. Experiments

We search and evaluate AMSNet and SPPLoss on the ShanghaiTech [75], WorldExpo'10 [74], UCF_CC_50 [24] and UCF-QNRF [25] crowd counting datasets.

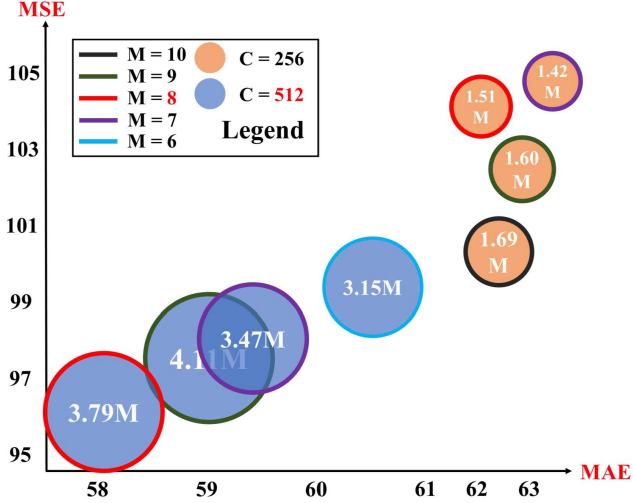


Figure 5. Illustrated hyper-parameter analysis. M is the number of extraction cells, C denotes the channels of feature map generated by the last extraction cell. Bottom left corner indicates superior counting result and the best parameters are colored in the legend.

4.1. Implementation Details

The original annotations provided by the datasets are coordinates pinpointing the location of each individual in the crowd. To soften these hard regression labels for better convergence, we apply a normalized 2D Gaussian filter to convert coordinate map into density map, on which each individual is represented by a Gaussian response with radius equals to 15 pixels [65].

4.1.1 Architecture Search

The architecture of AMSNet and SPPLoss, *i.e.* their corresponding architecture parameters $\alpha_{e,d,s}$ and $\beta_{e,d}$, are jointly searched on the split UCF-QNRF [25] training set. We choose to perform search on this dataset as it has the most challenging scenes with large crowd counts and density variations, and the search costs approximately 21 TITAN Xp GPU hours. Benefiting from the continuous relaxation, we optimize all architecture parameters and network weights w jointly using gradient descent. Specifically, the first-order optimization proposed in [37] is adopted, upon which w and α, β are optimized alternatively. For architecture parameters, we set the learning rate to be $6e-4$ with weight decay of $1e-3$. We follow the implementation as in [70, 34], where a warm-up training for network weights is first conducted for 40 epochs and stops the search early at 80 epochs. For training the network weights, we use a cosine learning rate that decays from 0.001 to 0.0004, and weight decay $1e-4$. Data augmentation with random sampling, flip and rotation are conducted to alleviate overfitting.

4.1.2 Architecture Training

After the architectures of AMSNet and SPPLoss are acquired by searching on the UCF-QNRF dataset, we re-train their network weights from scratch on each of the other datasets. We re-initialize the weights with Xavier initialization, and employ Adam with initial learning rate set to $1e-3$. This learning rate is decayed by 0.8 every 15K iterations.

4.1.3 Architecture Evaluation

Upon deployment, we directly feed images into AMSNet as a whole without patching, aiming to obtain high-quality density maps free from boundary artifacts. In counting-by-density, the crowd count on an estimated density map equals to the summation of all pixels, and to evaluate the counting performance we employ the mean average error (MAE) and the mean squared error (MSE) metrics:

$$MAE = \frac{1}{T} \sum_{i=1}^T |C_i - C_i^{gt}| \quad (5)$$

$$MSE = \sqrt{\frac{1}{T} \sum_{i=1}^T |C_i - C_i^{gt}|^2} \quad (6)$$

here T is the number of images in the test set, C_i and C_i^{gt} represent the predicted and ground truth counts of the i -th image. We also utilize the PSNR (Peak Signal-to-Noise Ratio) and SSIM (Structural Similarity in Image) metrics to evaluate density map quality. [56].

4.2. Search Result Analysis

The best searched multi-scale feature extraction and fusion cells, as well as the SPPLoss architecture are illustrated in Figure 4. As shown, extraction cell maintains the spatial and channel dimensions unchanged (1×1 convolutions are employed to manipulate the channel dimensions in the cells). The extraction cell primarily exploits dilated convolutions over normal ones, conforming to the fact that in the absence of heavy down-samplings, pixel-level models rely on dilations to enlarge receptive fields. Furthermore, different kernel sizes are employed in the extraction cell, showing its multi-scale capability in addressing scale variations. By taking in three encoded features and generating one output map, the fusion cell constitutes a multi-path decoding hierarchy, wherein primarily non-dilated convolutions with smaller kernels are selected to aggregate features more precisely and parameter-friendly. In addition, the deployed skip connections and varied kernels contribute to the decoder multi-scale capability.

Table 1. Estimation errors on the ShanghaiTech, the UCF_CC_50, and the UCF-QNRF datasets.

Method	ShanghaiTech Part_A		ShanghaiTech Part_B		UCF_CC_50		UCF-QNRF	
	MAE↓	MSE↓	MAE↓	MSE↓	MAE↓	MSE↓	MAE↓	MSE↓
Zhang <i>et al.</i> [74]	181.8	277.7	32.0	49.8	467.0	498.5	-	-
MCNN [75]	110.2	173.2	26.4	41.3	377.6	509.1	277	426
CP-CNN [56]	73.6	106.4	20.1	30.1	295.8	320.9	-	-
CSRNet [31]	68.2	115.0	10.6	16.0	266.1	397.5	-	-
SANet [10]	67.0	104.5	8.4	13.6	258.4	334.9	-	-
TEDNet [26]	64.2	109.1	8.2	12.8	249.4	354.5	113	188
ANF [73]	63.9	99.4	8.3	13.2	250.2	340.0	110	174
PACNN+ [55]	62.4	102.0	7.6	11.8	241.7	320.7	-	-
CAN [39]	62.3	100.0	7.8	12.2	212.2	243.7	107	183
AMSNet	58.0	96.2	7.1	10.4	208.6	296.3	103	165

Table 2. Model size and performance comparison among state-of-the-art counting methods on the ShanghaiTech Part_A.

Method	MAE↓	PSNR↑	SSIM↑	Size
MCNN [75]	110.2	21.4	0.52	0.13M
Switch-CNN [53]	90.4	-	-	15.11M
CP-CNN [56]	73.6	21.72	0.72	68.4M
CSRNet [31]	68.2	23.79	0.76	16.26M
SANet [10]	67.0	-	-	0.91M
TEDNet [26]	64.2	25.88	0.83	1.63M
ANF [73]	63.9	24.1	0.78	7.9M
AMSNet	58.0	26.96	0.89	3.79M
AMSNet_light	61.8	25.93	0.84	1.51M

4.3. Ablation Study on Searched Architectures

For ablation purposes, we employ the architecture proposed in [10] as the baseline encoder (composed of four inception-like blocks). The baseline decoder cascades two 3×3 convolutions interleaved with nearest-neighbor interpolation layers. The normal MSE loss is utilized as baseline supervision. By ablating different modules with its baseline, the ablation study result on the ShanghaiTech Part_A dataset is reported in Table 3. This table is partitioned into three groups row-wise, and each row indicates a specific configuration. The MAE and PSNR metrics are used to show the counting accuracy and density map quality.

Architectures in the first two groups (four rows) are optimized with the normal MSE loss. As shown, the searched AMSNet encoder improve counting accuracy and density map quality by 12.0% and 7.8%, while the searched decoder brings 8.5% and 1.7% improvements respectively. In the third group, AMSNet is supervised by different loss functions to demonstrate their efficacy. The Spatial Abstraction Loss (SAL) proposed in [26] adopts a hand-designed pyramidal architecture, which surpasses the normal MSE supervision on both counting and density estimation perfor-

Table 3. Ablation study results. Best performance is bolded, and arrows indicate the favorable directions of the metric values.

Configurations			MAE↓	PSNR↑
Encoder Architecture	1	Baseline Encoder Baseline Decoder	69.1	23.54
	2	AMSNet Encoder Baseline Decoder	60.8	25.52
Decoder Architecture	1	Baseline Encoder Baseline Decoder	69.1	23.54
	3	Baseline Encoder AMSNet Decoder	63.2	23.94
Supervision	3	AMSNet + MSE	59.4	25.96
	4	AMSNet + SAL	58.7	26.20
	5	AMSNet + SPPLoss	58.0	26.96

mance. These improvements are further enhanced by deploying SPPLoss, showing that the searched pyramid benefits counting and density estimation by supervising multi-scale structural information.

4.4. Hyper-parameter Study

Due to the heavy deployment of the extraction cell, the size and performance of AMSNet are largely dependent on two hyper-parameter M and C , each denoting the number of extraction cell and its output channel dimension. As illustrated in Figure 5, $M = 8$ and $C = 512$ render the best counting performance, but populate AMSNet with 3.79M parameters. When decreasing C to 256, the size of AMSNet also shrinks dramatically, but at the expense of decreased accuracy. Nevertheless, $M = 8$ still produces the best MAE in this case. As a result, we configure our AMSNet with $M = 8, C = 512$, and also maintain an AMSNet_light with $M = 8, C = 256$ in the experiment.

We compare the counting accuracy and density map quality of both AMSNet and AMSNet_light with other state-of-the-art counting methods in Table 2. As shown, AMSNet reports the best MAE and PSNR overall, while being heavier than three other methods. AMSNet_light, on

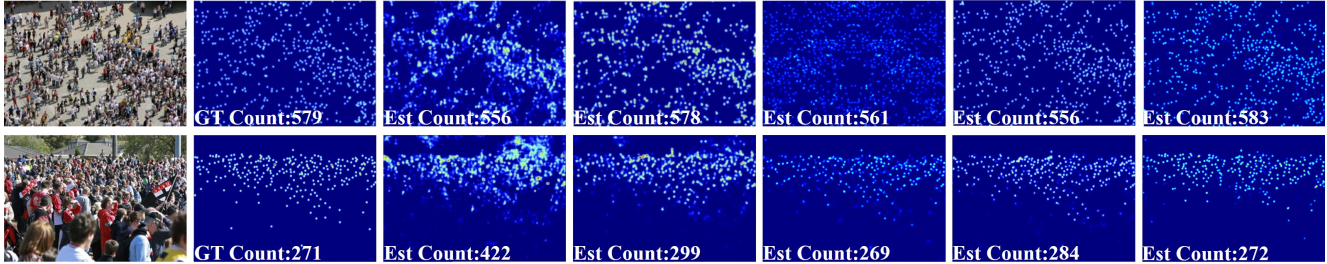


Figure 6. Visualization of density maps generated by state-of-the-art methods. The first two columns show inputs and the corresponding ground truth. As follows, the outputs of MCNN [75], SANet [10], TEDNet [26], ANF [73], and AMSNet are demonstrated in each column.

Table 4. The MAE comparison on WorldExpo’10.

Method	S1	S2	S3	S4	S5	Ave.
MCNN [75]	3.4	20.6	12.9	13.0	8.1	11.6
SANet [10]	2.6	13.2	9.0	13.3	3.0	8.2
CAN [39]	2.9	12.0	10.0	7.9	4.3	7.4
ECAN [39]	2.4	9.4	8.8	11.2	4.0	7.2
TEDNet [26]	2.3	10.1	11.3	13.8	2.6	8.0
AT-CSRNet [76]	1.8	13.7	9.2	10.4	3.7	7.8
AMSNet	1.6	8.8	10.8	10.4	2.5	6.8

the other hand, is the third most light model and achieves the best performance with the exception of AMSNet.

4.5. Performance and Comparison

We compare the counting-by-density performance of NAS-Count with other state-of-the-art methods on four challenging datasets. In particular, the counting accuracy comparison is reported in Tables 1 and 4, while the density map quality result is shown in Table 2.

4.5.1 Counting Accuracy

ShanghaiTech. The ShanghaiTech is composed of Part_A and Part_B with in total of 1198 images. It is one of the largest and most widely used datasets in crowd counting. As shown in Table 1, AMSNet leads others on ShanghaiTech in terms of both MAE and MSE. On Part_A, we surpass the second best by 6.9% and 3.2% in MAE and MSE. On Part_B we achieve 6.6% and 11.9% improvements respectively.

UCF_CC_50 The UCF_CC_50 dataset contains 50 images of varying resolutions and densities. In consideration of sample scarcity, we follow the standard protocol [24] and use 5-fold cross-validation to evaluate method performance. As shown in Table 1, AMSNet achieves the best MAE and second MSE, elevating the MAE performance by 1.7%.

UCF-QNRF The UCF-QNRF dataset introduced by Idress *et al.* [25] has images with the highest crowd counts and largest density variation, ranging from 49 to 12865 people per image. These characteristics make UCF-QNRF ex-

remely challenging for counting models, and only selected methods have published their results. Nonetheless, we produce the best MAE and MSE scores on this dataset, leading the second best by 3.7% and 5.2%.

WorldExpo’10 The WorldExpo’10 dataset [74] contains 3980 images covering 108 different scenes. The training set contains 3380 images, and the test set includes 600 frames from 5 different scenes. As shown in Table 4, AMSNet achieves the lowest average MAE over five scenes, and also performs the best on the three scenes individually.

4.5.2 Density Map Quality

As shown in Table 2, we employ PSNR and SSIM indices to compare the quality of density maps estimated by different methods, and AMSNet performs the best on both indices, outperforming the second best by 4.0% and 6.7%. Notably, even by deploying AMSNet.light which is the third lightest model, we still generate the most high-quality density map. Quantitatively, density maps produced by MCNN [75], SANet [10], TEDNet [26], ANF [73], and our AMSNet on ShanghaiTech Part_A are displayed in Figure 6. We further showcase more density maps generated by AMSNet on all employed datasets in Figure 3.

5. Conclusion

NAS-Count is the first endeavor introducing neural architecture search into counting-by-density. In this paper, we developed the state-of-the-art AMSNet encoder-decoder as well as the SPPLoss supervision paradigm. Specifically, AMSNet employs a novel composition of multi-scale feature extraction and fusion cells, which are both searched efficiently from a counting-specific search space using gradient-based strategy. SPPLoss extends normal MSE loss with a scale pyramid architecture, which helps to supervise structural information in the density map at multiple scales. By jointly searching AMSNet and SPPLoss end-to-end, NAS-Count surpasses tedious hand-designing efforts by achieving a multi-scaled model automatically with less than 1 GPU day, and demonstrates overall the best performance on four challenging datasets.

References

- [1] Bowen Baker, Otkrist Gupta, Nikhil Naik, and Ramesh Raskar. Designing neural network architectures using reinforcement learning. *arXiv preprint arXiv:1611.02167*, 2016. **3**
- [2] Bowen Baker, Otkrist Gupta, Ramesh Raskar, and Nikhil Naik. Accelerating neural architecture search using performance prediction. *arXiv preprint arXiv:1705.10823*, 2017. **3**
- [3] Gabriel Bender, Pieter-Jan Kindermans, Barret Zoph, Vijay Vasudevan, and Quoc Le. Understanding and simplifying one-shot architecture search. In *International Conference on Machine Learning*, pages 549–558, 2018. **3**
- [4] James Bergstra and Yoshua Bengio. Random search for hyper-parameter optimization. *Journal of Machine Learning Research*, 13(Feb):281–305, 2012. **3**
- [5] Lokesh Boominathan, Srinivas SS Kruthiventi, and R Venkatesh Babu. Crowdnet: A deep convolutional network for dense crowd counting. In *Proceedings of the 2016 ACM on Multimedia Conference*, pages 640–644. ACM, 2016. **2**
- [6] Andrew Brock, Theodore Lim, James M Ritchie, and Nick Weston. Smash: one-shot model architecture search through hypernetworks. *arXiv preprint arXiv:1708.05344*, 2017. **3**
- [7] Michael M Bronstein, Joan Bruna, Yann LeCun, Arthur Szlam, and Pierre Vandergheynst. Geometric deep learning: going beyond euclidean data. *IEEE Signal Processing Magazine*, 34(4):18–42, 2017. **1**
- [8] Han Cai, Tianyao Chen, Weinan Zhang, Yong Yu, and Jun Wang. Efficient architecture search by network transformation. In *Proceedings of the AAAI Conference on Artificial Intelligence*, 2018. **3**
- [9] Han Cai, Ligeng Zhu, and Song Han. Proxylessnas: Direct neural architecture search on target task and hardware. *arXiv preprint arXiv:1812.00332*, 2018. **3**
- [10] Xinkun Cao, Zhipeng Wang, Yanyun Zhao, and Fei Su. Scale aggregation network for accurate and efficient crowd counting. In *Proceedings of the European Conference on Computer Vision*, pages 734–750, 2018. **1, 2, 5, 7, 8**
- [11] Antoni B Chan and Nuno Vasconcelos. Bayesian poisson regression for crowd counting. In *Proceedings of the International Conference on Computer Vision*, pages 545–551, 2009. **2**
- [12] Ke Chen, Chen Change Loy, Shaogang Gong, and Tony Xiang. Feature mining for localised crowd counting. In *Proceedings of the British Machine Vision Conference*, volume 1, page 3, 2012. **1**
- [13] Liang-Chieh Chen, Maxwell Collins, Yukun Zhu, George Papandreou, Barret Zoph, Florian Schroff, Hartwig Adam, and Jon Shlens. Searching for efficient multi-scale architectures for dense image prediction. In *Proceedings of the Advances in Neural Information Processing Systems*, pages 8699–8710, 2018. **2, 3**
- [14] Liang-Chieh Chen, George Papandreou, Iasonas Kokkinos, Kevin Murphy, and Alan L Yuille. Deeplab: Semantic image segmentation with deep convolutional nets, atrous convolution, and fully connected crfs. *IEEE Transactions on Pattern Analysis and Machine Intelligence*, 40(4):834–848, 2017. **5**
- [15] Xin Chen, Lingxi Xie, Jun Wu, and Qi Tian. Progressive differentiable architecture search: Bridging the depth gap between search and evaluation. *arXiv preprint arXiv:1904.12760*, 2019. **3**
- [16] Yukang Chen, Tong Yang, Xiangyu Zhang, Gaofeng Meng, Chunhong Pan, and Jian Sun. Detnas: Neural architecture search on object detection. *arXiv preprint arXiv:1903.10979*, 2019. **3**
- [17] Piotr Dollar, Christian Wojek, Bernt Schiele, and Pietro Perona. Pedestrian detection: An evaluation of the state of the art. *IEEE Transactions on Pattern Analysis and Machine Intelligence*, 34(4):743–761, 2012. **2**
- [18] Thomas Elsken, Jan-Hendrik Metzen, and Frank Hutter. Simple and efficient architecture search for convolutional neural networks. *arXiv preprint arXiv:1711.04528*, 2017. **3**
- [19] Thomas Elsken, Jan Hendrik Metzen, and Frank Hutter. Neural architecture search: A survey. *Journal of Machine Learning Research*, 20(55):1–21, 2019. **2**
- [20] Luca Fiaschi, Ullrich Köthe, Rahul Nair, and Fred A Hamprecht. Learning to count with regression forest and structured labels. In *Proceedings of the International Conference on Pattern Recognition*, pages 2685–2688. IEEE, 2012. **2**
- [21] Weina Ge and Robert T Collins. Marked point processes for crowd counting. In *Proceedings of the IEEE Conference on Computer Vision and Pattern Recognition*, pages 2913–2920, 2009. **1, 2**
- [22] Golnaz Ghiasi, Tsung-Yi Lin, and Quoc V Le. Nas-fpn: Learning scalable feature pyramid architecture for object detection. In *Proceedings of the IEEE Conference on Computer Vision and Pattern Recognition*, pages 7036–7045, 2019. **3**
- [23] Daniel Golovin, Benjamin Solnik, Subhodeep Moitra, Greg Kochanski, John Karro, and D Sculley. Google vizier: A service for black-box optimization. In *Proceedings of the 23rd ACM SIGKDD International Conference on Knowledge Discovery and Data Mining*, pages 1487–1495. ACM, 2017. **3**
- [24] Haroon Idrees, Imran Saleemi, Cody Seibert, and Mubarak Shah. Multi-source multi-scale counting in extremely dense crowd images. In *Proceedings of the IEEE Conference on Computer Vision and Pattern Recognition*, pages 2547–2554, 2013. **1, 2, 5, 8**
- [25] Haroon Idrees, Muhammad Tayyab, Kishan Athrey, Dong Zhang, Somaya Al-Maadeed, Nasir Rajpoot, and Mubarak Shah. Composition loss for counting, density map estimation and localization in dense crowds. *arXiv preprint arXiv:1808.01050*, 2018. **1, 2, 5, 6, 8**
- [26] Xiaolong Jiang, Zehao Xiao, Baochang Zhang, Xiantong Zhen, Xianbin Cao, David Doermann, and Ling Shao. Crowd counting and density estimation by trellis encoder-decoder networks. In *Proceedings of the IEEE Conference on Computer Vision and Pattern Recognition*, pages 6133–6142, 2019. **1, 2, 5, 7, 8**
- [27] Di Kang, Zheng Ma, and Antoni B Chan. Beyond counting: comparisons of density maps for crowd analysis tasks—counting, detection, and tracking. *IEEE Transactions on Circuits and Systems for Video Technology*, 2018. **2**

- [28] Shohei Kumagai, Kazuhiro Hotta, and Takio Kurita. Mixture of counting cnns: Adaptive integration of cnns specialized to specific appearance for crowd counting. *arXiv preprint arXiv:1703.09393*, 2017. [2](#)
- [29] Victor Lempitsky and Andrew Zisserman. Learning to count objects in images. In *Proceedings of the Advances in Neural Information Processing Systems*, pages 1324–1332, 2010. [1](#), [2](#)
- [30] Min Li, Zhaoxiang Zhang, Kaiqi Huang, and Tieniu Tan. Estimating the number of people in crowded scenes by mid based foreground segmentation and head-shoulder detection. In *Proceedings of the International Conference on Pattern Recognition*, pages 1–4. IEEE, 2008. [1](#), [2](#)
- [31] Yuhong Li, Xiaofan Zhang, and Deming Chen. Csrnet: Dilated convolutional neural networks for understanding the highly congested scenes. In *Proceedings of the IEEE Conference on Computer Vision and Pattern Recognition*, pages 1091–1100, 2018. [2](#), [5](#), [7](#)
- [32] Hanwen Liang, Shifeng Zhang, Jiacheng Sun, Xingqiu He, Weiran Huang, Kechen Zhuang, and Zhenguo Li. Darts+: Improved differentiable architecture search with early stopping. *arXiv preprint arXiv:1909.06035*, 2019. [3](#)
- [33] Guosheng Lin, Anton Milan, Chunhua Shen, and Ian D Reid. Refinenet: Multi-path refinement networks for high-resolution semantic segmentation. In *Proceedings of the IEEE Conference on Computer Vision and Pattern Recognition*, volume 1, page 5, 2017. [2](#)
- [34] Chenxi Liu, Liang-Chieh Chen, Florian Schroff, Hartwig Adam, Wei Hua, Alan L Yuille, and Li Fei-Fei. Auto-deeplab: Hierarchical neural architecture search for semantic image segmentation. In *Proceedings of the IEEE Conference on Computer Vision and Pattern Recognition*, pages 82–92, 2019. [2](#), [3](#), [6](#)
- [35] Chenxi Liu, Barret Zoph, Maxim Neumann, Jonathon Shlens, Wei Hua, Li-Jia Li, Li Fei-Fei, Alan Yuille, Jonathan Huang, and Kevin Murphy. Progressive neural architecture search. In *Proceedings of the European Conference on Computer Vision*, pages 19–34, 2018. [1](#), [3](#)
- [36] Hanxiao Liu, Karen Simonyan, Oriol Vinyals, Chrisantha Fernando, and Koray Kavukcuoglu. Hierarchical representations for efficient architecture search. *arXiv preprint arXiv:1711.00436*, 2017. [3](#)
- [37] Hanxiao Liu, Karen Simonyan, and Yiming Yang. Darts: Differentiable architecture search. *arXiv preprint arXiv:1806.09055*, 2018. [2](#), [3](#), [4](#), [6](#)
- [38] Lingbo Liu, Zhilin Qiu, Guanbin Li, Shufan Liu, Wanli Ouyang, and Liang Lin. Crowd counting with deep structured scale integration network. In *Proceedings of the International Conference on Computer Vision*, pages 1774–1783, 2019. [2](#)
- [39] Weizhe Liu, Mathieu Salzmann, and Pascal Fua. Context-aware crowd counting. In *Proceedings of the IEEE Conference on Computer Vision and Pattern Recognition*, June 2019. [2](#), [7](#), [8](#)
- [40] Xialei Liu, Joost van de Weijer, and Andrew D Bagdanov. Leveraging unlabeled data for crowd counting by learning to rank. *arXiv preprint arXiv:1803.03095*, 2018. [1](#)
- [41] Risto Miikkulainen, Jason Liang, Elliot Meyerson, Aditya Rawal, Daniel Fink, Olivier Francon, Bala Raju, Hormoz Shahrzad, Arshak Navruzyan, Nigel Duffy, et al. Evolving deep neural networks. In *Artificial Intelligence in the Age of Neural Networks and Brain Computing*, pages 293–312. Elsevier, 2019. [3](#)
- [42] Vladimir Nekrasov, Hao Chen, Chunhua Shen, and Ian Reid. Fast neural architecture search of compact semantic segmentation models via auxiliary cells. In *Proceedings of the IEEE Conference on Computer Vision and Pattern Recognition*, pages 9126–9135, 2019. [2](#), [3](#)
- [43] Vladimir Nekrasov, Chunhua Shen, and Ian Reid. Lightweight refinenet for real-time semantic segmentation. *arXiv preprint arXiv:1810.03272*, 2018. [2](#)
- [44] Daniel Onoro-Rubio and Roberto J López-Sastre. Towards perspective-free object counting with deep learning. In *Proceedings of the European Conference on Computer Vision*, pages 615–629. Springer, 2016. [1](#), [2](#)
- [45] Hieu Pham, Melody Y Guan, Barret Zoph, Quoc V Le, and Jeff Dean. Efficient neural architecture search via parameter sharing. *arXiv preprint arXiv:1802.03268*, 2018. [3](#)
- [46] E Real, A Aggarwal, Y Huang, and QV Le. Aging evolution for image classifier architecture search. In *Proceedings of the AAAI Conference on Artificial Intelligence*, 2019. [1](#), [3](#)
- [47] Esteban Real, Alok Aggarwal, Yanping Huang, and Quoc V Le. Regularized evolution for image classifier architecture search. In *Proceedings of the AAAI Conference on Artificial Intelligence*, volume 33, pages 4780–4789, 2019. [1](#), [3](#)
- [48] Esteban Real, Sherry Moore, Andrew Selle, Saurabh Saxena, Yutaka Leon Suematsu, Jie Tan, Quoc V Le, and Alexey Kurakin. Large-scale evolution of image classifiers. In *Proceedings of the 34th International Conference on Machine Learning-Volume 70*, pages 2902–2911. JMLR. org, 2017. [1](#), [2](#), [3](#)
- [49] Olaf Ronneberger, Philipp Fischer, and Thomas Brox. U-net: Convolutional networks for biomedical image segmentation. In *Proceedings of the International Conference on Medical Image Computing and Computer-assisted Intervention*, pages 234–241. Springer, 2015. [2](#)
- [50] David Ryan, Simon Denman, Clinton Fookes, and Sridha Sridharan. Crowd counting using multiple local features. In *Digital Image Computing: Techniques and Applications, 2009. DICTA'09.*, pages 81–88. IEEE, 2009. [2](#)
- [51] David Ryan, Simon Denman, Sridha Sridharan, and Clinton Fookes. An evaluation of crowd counting methods, features and regression models. *Computer Vision and Image Understanding*, 130:1–17, 2015. [1](#), [2](#)
- [52] Sami Abdulla Mohsen Saleh, Shahrel Azmin Suandi, and Haidi Ibrahim. Recent survey on crowd density estimation and counting for visual surveillance. *Engineering Applications of Artificial Intelligence*, 41:103–114, 2015. [1](#), [2](#)
- [53] Deepak Babu Sam, Shiv Surya, and R Venkatesh Babu. Switching convolutional neural network for crowd counting. In *Proceedings of the IEEE Conference on Computer Vision and Pattern Recognition*, volume 1, page 6, 2017. [1](#), [7](#)
- [54] Shreyas Saxena and Jakob Verbeek. Convolutional neural fabrics. In *Proceedings of the Advances in Neural Information Processing Systems*, pages 4053–4061, 2016. [2](#), [3](#)

- [55] Miaojing Shi, Zhaohui Yang, Chao Xu, and Qijun Chen. Revisiting perspective information for efficient crowd counting. In *Proceedings of the IEEE Conference on Computer Vision and Pattern Recognition*, pages 7279–7288, 2019. 7
- [56] Vishwanath A Sindagi and Vishal M Patel. Generating high-quality crowd density maps using contextual pyramid cnns. In *Proceedings of the International Conference on Computer Vision*, pages 1879–1888. IEEE, 2017. 6, 7
- [57] Vishwanath A Sindagi and Vishal M Patel. A survey of recent advances in cnn-based single image crowd counting and density estimation. *Pattern Recognition Letters*, 107:3–16, 2018. 1, 2
- [58] David R So, Chen Liang, and Quoc V Le. The evolved transformer. *arXiv preprint arXiv:1901.11117*, 2019. 3
- [59] Dimitrios Stamoulis, Ruizhou Ding, Di Wang, Dimitrios Lymberopoulos, Bodhi Priyantha, Jie Liu, and Diana Marculescu. Single-path nas: Designing hardware-efficient convnets in less than 4 hours. *arXiv preprint arXiv:1904.02877*, 2019. 3
- [60] Kenneth O Stanley and Risto Miikkulainen. Evolving neural networks through augmenting topologies. *Evolutionary Computation*, 10(2):99–127, 2002. 3
- [61] Mingxing Tan, Bo Chen, Ruoming Pang, Vijay Vasudevan, Mark Sandler, Andrew Howard, and Quoc V Le. Mnasnet: Platform-aware neural architecture search for mobile. In *Proceedings of the IEEE Conference on Computer Vision and Pattern Recognition*, pages 2820–2828, 2019. 3
- [62] Elad Walach and Lior Wolf. Learning to count with cnn boosting. In *Proceedings of the European Conference on Computer Vision*, pages 660–676. Springer, 2016. 2
- [63] Meng Wang and Xiaogang Wang. Automatic adaptation of a generic pedestrian detector to a specific traffic scene. In *Proceedings of the IEEE Conference on Computer Vision and Pattern Recognition*, pages 3401–3408, 2011. 2
- [64] Qi Wang, Junyu Gao, Wei Lin, and Yuan Yuan. Learning from synthetic data for crowd counting in the wild. In *Proceedings of the The IEEE Conference on Computer Vision and Pattern Recognition*, June 2019. 2
- [65] Ze Wang, Zehao Xiao, Kai Xie, Qiang Qiu, Xiantong Zhen, and Xianbin Cao. In defense of single-column networks for crowd counting. *arXiv preprint arXiv:1808.06133*, 2018. 2, 6
- [66] Lingxi Xie and Alan Yuille. Genetic cnn. In *Proceedings of the International Conference on Computer Vision*, pages 1379–1388, 2017. 3
- [67] Saining Xie, Alexander Kirillov, Ross Girshick, and Kaiming He. Exploring randomly wired neural networks for image recognition. *arXiv preprint arXiv:1904.01569*, 2019. 1
- [68] Sirui Xie, Hehui Zheng, Chunxiao Liu, and Liang Lin. Snas: stochastic neural architecture search. *arXiv preprint arXiv:1812.09926*, 2018. 3
- [69] Hang Xu, Lewei Yao, Wei Zhang, Xiaodan Liang, and Zhen-guo Li. Auto-fpn: Automatic network architecture adaptation for object detection beyond classification. In *Proceedings of the International Conference on Computer Vision*, pages 6649–6658, 2019. 3
- [70] Yuhui Xu, Lingxi Xie, Xiaopeng Zhang, Xin Chen, Guo-Jun Qi, Qi Tian, and Hongkai Xiong. Pc-darts: Partial channel connections for memory-efficient differentiable architecture search. *arXiv preprint arXiv:1907.05737*, 2019. 2, 3, 4, 6
- [71] Jing Yang, Qingshan Liu, and Kaihua Zhang. Stacked hour-glass network for robust facial landmark localisation. In *Proceedings of the IEEE Conference on Computer Vision and Pattern Recognition Workshops*, pages 2025–2033. IEEE, 2017. 2
- [72] Chris Ying, Aaron Klein, Esteban Real, Eric Christiansen, Kevin Murphy, and Frank Hutter. Nas-bench-101: Towards reproducible neural architecture search. *arXiv preprint arXiv:1902.09635*, 2019. 2
- [73] Anran Zhang, Lei Yue, Jiayi Shen, Fan Zhu, Xiantong Zhen, Xianbin Cao, and Ling Shao. Attentional neural fields for crowd counting. In *Proceedings of the International Conference on Computer Vision*, October 2019. 7, 8
- [74] Cong Zhang, Hongsheng Li, Xiaogang Wang, and Xiaokang Yang. Cross-scene crowd counting via deep convolutional neural networks. In *Proceedings of the IEEE Conference on Computer Vision and Pattern Recognition*, pages 833–841, 2015. 2, 5, 7, 8
- [75] Yingying Zhang, Desen Zhou, Siqin Chen, Shenghua Gao, and Yi Ma. Single-image crowd counting via multi-column convolutional neural network. In *Proceedings of the IEEE Conference on Computer Vision and Pattern Recognition*, pages 589–597, 2016. 1, 2, 5, 7, 8
- [76] Muming Zhao, Jian Zhang, Chongyang Zhang, and Wenjun Zhang. Leveraging heterogeneous auxiliary tasks to assist crowd counting. In *Proceedings of the IEEE Conference on Computer Vision and Pattern Recognition*, June 2019. 2, 8
- [77] Barret Zoph and Quoc V Le. Neural architecture search with reinforcement learning. *arXiv preprint arXiv:1611.01578*, 2016. 1, 2, 3
- [78] Barret Zoph, Vijay Vasudevan, Jonathon Shlens, and Quoc V Le. Learning transferable architectures for scalable image recognition. In *Proceedings of the IEEE Conference on Computer Vision and Pattern Recognition*, pages 8697–8710, 2018. 1, 3